

# Advanced Virtual Corrective Osteotomy

André Neubauer<sup>a,\*</sup>, Katja Bühler<sup>a</sup>, Rainer Wegenkittl<sup>b</sup>,  
Andreas Rauchberger<sup>b</sup>, Michael Rieger<sup>c</sup>

<sup>a</sup> *Research Center for Virtual Reality and Visualization, Vienna, Austria*

<sup>b</sup> *Tiani Medgraph, Vienna, Austria*

<sup>c</sup> *Department of Radiology, Innsbruck University Hospital, Innsbruck, Austria*

---

**Abstract.** This paper presents a new software system for preoperative planning and intraoperative support for corrective osteotomy. Patients with a malunited fracture of the distal radius undergo a surgical intervention in which the radius is cut into two segments and the distal segment is repositioned. The osteotomy is first carried out virtually. The products of this process are templates which, using a navigation system and intraoperative radiological imaging, guide the physical osteotomy.

*Keywords:* corrective osteotomy; preoperative planning; intraoperative support

---

## 1. Purpose

Fractures of the distal radius are among the most common of all orthopedic injuries. As explained in an earlier publication [8], patients with malunited distal radius fracture and therefore severe limitation of wrist motion range undergo a corrective intervention called *distal radius osteotomy*. During this procedure, the radius is cut into two fragments, the *proximal radius fragment* and the *distal radius fragment*. The distal radius fragment is repositioned to its original state, i.e., as it was before the fracture (see Figure 1, left image).

The procedure requires careful planning of the restoration of angles and length of the distal radius to guarantee normal function. Due to the missing spatial component, traditional 2D planning techniques using x-ray images, pen and ruler have major limitations with respect to rearrangement and reorientation of spatial objects and the correct intra-operative realization of a pre-operative plan.

In the late 80s, computer assisted planning of distal radius osteotomy was proposed by Bilic and Zdravcovic to overcome these drawbacks [2, 3, 9]. The system used a virtual 3D model of wrist and forearm reconstructed out of two orthogonal x-ray images and applied computer aided design (CAD) principles for the planning step. Jupiter et al. used CT images and CAD/CAM techniques to produce real one-to-one 3D models of complex malunions for preoperative planning [7]. Ellis et al. [1, 5] proposed the first system that provides a tool for virtual preoperative planning of distal radius osteotomy based on CT data and intraoperative support for correct translation of the plan to the patient.

---

\* Corresponding author. *E-mail address:* neubauer@vrvis.at.

This paper introduces a new software system enabling intuitive preoperative planning and intraoperative support for corrective osteotomy. Repositioning is first carried out virtually using the software. This process creates templates used intraoperatively both to determine the correct target location of cutting the radius and to guide and assess physical repositioning.

## 2. Methods

The following paragraphs enumerate the steps of the virtual procedure. All functionality apart from step 5 was integrated into the JVision workstation by Tiani Medgraph (<http://www.tiani.com>).

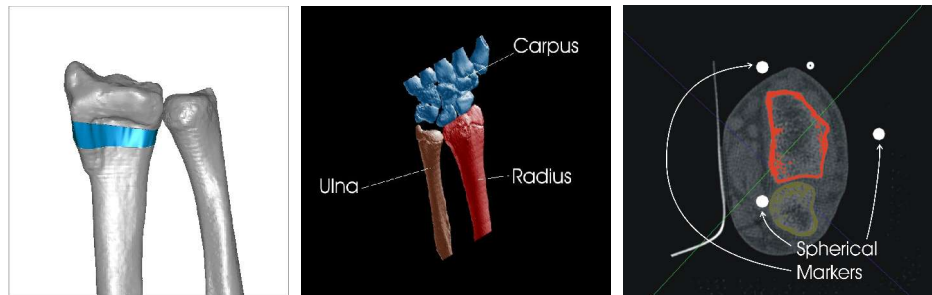


Fig. 1. Left: The reconstructed radius after virtual relocation of the distal radius segment, here a repositioning device (blue) is indicated. Center: The result of segmentation. Right: Spherical markers indicating the correct cutting plane.

### 2.0 Data Acquisition

Both the involved and the contralateral forearm and wrist are examined with a multislice CT (LightSpeed Qx/i, GE, Milwaukee) using 1.25 mm collimation, the High Quality Mode (pitch 3), a reconstruction interval of 0.6 mm and the bone reconstruction kernel.

### 2.1 Segmentation

In this step, the CT image of the involved forearm and wrist is segmented to extract radius, ulna and carpus. Three binary segmentation masks are generated representing these three objects (see Figure 1, center image).

The first segmentation step is thresholding. This step creates a single object containing all voxels whose values exceed a user-defined threshold. Now this object must be separated into the three individual segments (ulna, radius and carpus). Usually, even if an appropriate threshold has been chosen, two or more segments are connected, i.e., there exists at least one 26-connected path from any voxel of one segment to any voxel of the other segment traversing only voxels that are inside the segmented object. In this case, separating the two segments correctly is not a trivial task. In the presented system, the user can select a voxel located on the boundary between the two segments and initiate a watershed-based segmentation algorithm that automatically performs the separation. In case of inaccuracies, manual corrections are performed. The boundaries of the resulting

objects can be slightly smoothed, using an error bound, in order to reduce the impact of noise within the CT data.

The contralateral, healthy forearm is segmented as well. Here only one object is generated, representing the complete forearm skeleton. Therefore a thresholding operation is sufficient.

## 2.2 Definition of the cutting plane

Next, the user selects the plane at which to cut the malunited radius. User interaction takes place via a multi-planar reconstruction (MPR) displaying the CT data along three mutually orthogonal cross-sections through the volume (see Figure 2). The planes defining these sections can be arbitrarily rotated by the user. Also each section can be arbitrarily moved parallel to its normal. The intersection of any pair of MPR sections is depicted in both sections. In the MPR, voxels belonging to segmented objects are colored accordingly. This tool is a powerful and intuitive means of investigating the complete 3D volume. At any point in time, the user can select the current plane of one of the three MPR-sections to be used as the cutting plane. From this moment on, the intersection of the cutting plane with each MPR-section is displayed in the corresponding MPR section as a white line. Figure 2 shows the three sections of the MPR after the carrier plane of section 1 has been selected as the cutting plane. The cutting plane is therefore indicated by a white line in sections 2 and 3 of the MPR.

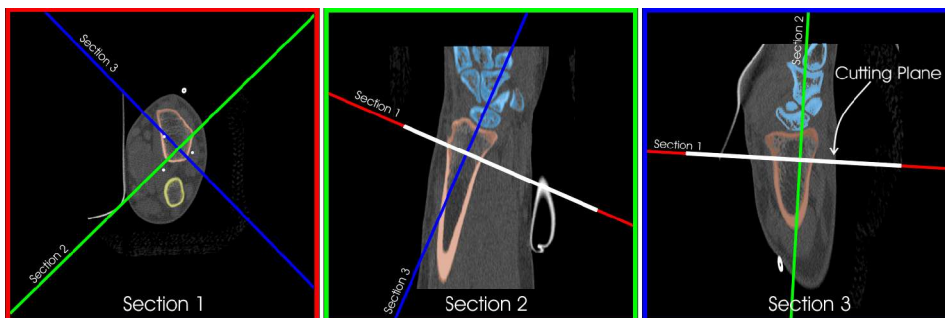


Fig. 2. The MPR after definition of the cutting plane. The plane of the left section (Section 1) has been chosen to be the cutting plane.

Using the MPR, the user can, after selection of the cutting plane, arbitrarily navigate through the volume and assess the correctness of the cutting plane. Figure 3 shows the same cutting plane as Figure 2, after some navigation in the MPR.

## 2.3 Virtually cutting the radius

The CT data can be virtually cut along the cutting plane selected as described in Section 2.2. The radius object is cut into two segments (see Figure 3), the proximal radius segment and the distal radius segment. This is done to facilitate virtual repositioning and generation of a data set serving as a template during the real procedure (see section 2.6). At both sides of the cutting plane, a thin (about 1 mm) layer of virtual bone tissue is

removed (see Figure 3). This is because also through cutting the real bone, a thin layer of bone tissue will be lost.

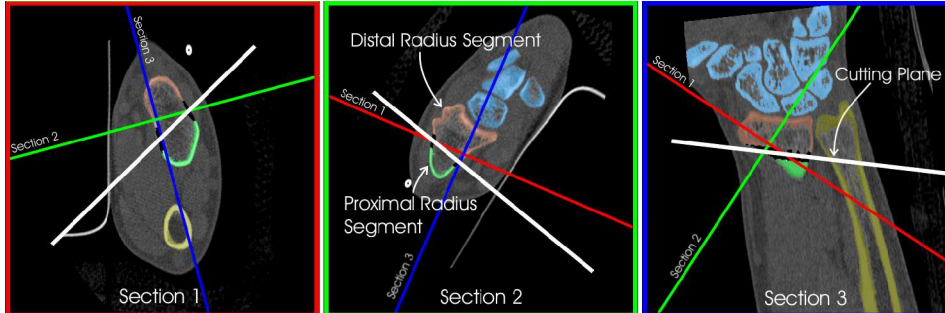


Fig. 3. The MPR after virtually cutting the radius.

The cutting plane is marked in the CT volume using three spherical markers of a user-specified diameter (see Figure 1, right image). These markers, centered on the cutting plane, are written to the CT data by changing the underlying voxel values to the maximum CT value (3071 Hounsfield Units). The resulting (marked) CT data can now be stored in the PACS. Intraoperatively, this modified data set is used to detect the correct cutting plane. A navigation system intraoperatively displays the plane indicated by the three markers, therefore indicating to the surgeon the plane along which to cut the radius.

#### 2.4 Generation of a polygonal mesh

After the radius has been cut, each object (ulna, carpus, proximal radius, distal radius and healthy forearm) is converted to a polygon model. We refer to segmented objects as 'binary objects', since each voxel either entirely belongs to an object, or not at all.

There are various ways of converting binary data to polygon models. We selected the *Surface Nets* method by Sarah Frisken Gibson et al.[4, 6] because it creates smooth surfaces which meet a given error bound and high-quality meshes with no degenerated triangles. However, to acquire polygonal models of high quality, we slightly adapted the algorithm proposed by Gibson. The original algorithm works as follows: A vertex is placed into each cell neighboring at least one voxel belonging to the binary object and at least one voxel not belonging to the object. In each of a number of relaxation steps, each vertex is moved towards the average position of its direct neighbors. A vertex is not allowed to cross the boundaries of the cell where it has originally been placed. After the relaxation, quadrilaterals are identified. If four cells sharing a common edge each contain a vertex, these four vertices are subsumed into a quadrilateral. Each quadrilateral is then split up into two triangles and added to the mesh.

It can be easily shown that this algorithm can lead to redundant triangles: Imagine, for example, a binary object that contains only two voxels which are located next to each other. The group of four cells sharing the edge connecting the two voxels is detected as a linked quadrilateral and therefore triangulated, although it does not represent a part of the object boundary. As a solution, we propose to triangulate a quadrilateral only if the edge shared by the four cells connects an object-voxel and a voxel not belonging to the binary

object. This yields also a second advantage: For further processing it is important that the mesh is waterproof, which includes the demand that the surface normals of all triangles point outwards, i.e., away from the object. The orientation of the surface normal of a triangle depends on the order in which its vertices are processed to compute the normal. If this order is initialized correctly before relaxation (such that the surface normal points towards the voxel which is not inside the object), it will remain correct even though the vertices are moved during the relaxation. Therefore, despite the fact that single triangles might completely change their orientations during relaxation, the normals will always correctly point outwards.

We also propose to improve the relaxation process: Each vertex is moved towards the average position of only those neighboring vertices that the vertex will later be connected to by at least one triangle. This tailors the relaxation process towards its goal - to smooth surfaces. If that optimization is not applied, disconnected parts of surfaces may be moved towards each other, which is not a desired effect.

Another adaptation is to confine the movement of each vertex to a region such that a given error bound is met, rather than to the boundaries of its cell. This not only results in a smoother surface, but has a second advantage: Usually CT volumes are anisotropic. Confining the movement of each vertex to a cell that is a cuboid, but in general no cube, allows more drastic movement into z-direction compared to x and y, which is an undesired effect.

### *2.5 Registration of both forearms*

The polygonal objects representing the involved forearm are registered (aligned) with the mirrored polygonal model of the healthy arm. The distal radius segment is repositioned such that it aligns with its counterpart in the healthy wrist. This step is performed using reverse engineering software (Raindrop Geomagic Studio). The movement of the distal radius as performed in this step is expressed via a transformation matrix and exported for further processing.

### *2.6 Application of the transformation to CT data*

The transformation matrix acquired in the previous step is applied to transform the object representing the distal radius segment. Together with the binary segmentation mask defining the object, the underlying CT data and the markers defining the cutting plane (see Section 2.3) are transformed according to the matrix. The resulting volume is exported as a new data set and can be used intraoperatively as a template. During the physical procedure, the distal radius segment will be repositioned such that the intraoperative radiological image corresponds to the transformed data. Transformation of the markers defining the cutting plane facilitates the repositioning - the navigation system depicts the transformed cutting plane and the surgeon aligns the distal radius segment with this plane.

### *2.7 Production of the repositioning device*

If no navigation system is used, as was the case until recently, instead of the template, a physical repositioning device [8] is used to correctly relocate the distal radius fragment

during the physical procedure is produced (see Figure 1, left image). For this, a new binary object connecting the two radius segments is generated. This object is then converted to a polygon mesh as described in step 4 and exported to a STL (stereo lithography) -file. Stereo lithography is applied to, from this data, generate the repositioning device.

### 3 Results

The usability of the software is currently being assessed within a number of tests. Preliminary results are very encouraging. The new software system substantially accelerates both preoperative planning and the surgical procedure. Precision during the physical procedure is significantly facilitated by the new planning tool, with the resulting radiological templates and navigation aids guiding the real osteotomy. The usage of the new software, along with a navigation system, can replace production of a physical repositioning device (see Section 2.7).

### 4 Conclusion

In the near future, the system will be further improved and evaluated. Early improvements will include significant reduction of user interaction during the segmentation process and the combination of all processing steps into one software tool.

### References:

- [1] G.S. Athwal, R.E. Ellis, C.F. Small, D.R. Pichora. Computer-assisted distal radius osteotomy. *J Hand Surg [Am]* 28(6):951-8. 2003
- [2] R. Bilic, V. Zdravkovic. Planning corrective osteotomy of the distal end of the radius. 2. Computer-aided planning and postoperative follow-up. *Unfallchirurg*. 91(12):575-80. 1988
- [3] R. Bilic, V. Zdravkovic, Z. Boljevic. Osteotomy for deformity of the radius. Computer-assisted three-dimensional modelling. *J Bone Joint Surg Br*. 76(1):150-4. 1994
- [4] P. W. de Bruin, F. Vos, F. H. Post, S. Frisken Gibson, A. M. Vossepoel. Improving Triangle Mesh Quality with Surface Nets. *Proceedings of the Third International Conference on Medical Image Computing and Computer-Assisted Intervention*, 2000
- [5] H. Croitoru, R.E. Ellis, R. Prihar, C.F. Small, D.R. Pichora. Fixation-based surgery: a new technique for distal radius osteotomy. *Comput Aided Surg*. 6(3):160-9. 2001
- [6] S. Frisken Gibson. Constrained elastic surface nets: generating smooth surfaces from binary segmented data. *Proceedings of Medical Image Computation and Computer Assisted Surgery*, 1998 (MICCAI '98)
- [7] J.B. Jupiter, J. Ruder, D.A. Roth. Computer-generated bone models in the planning of osteotomy of multidirectional distal radius malunions. *J Hand Surg [Am]*. 17(3):406-15. 1992
- [8] Michael Rieger, Ammar Mallouhi, Markus Gabl, Hannes Gruber, Reto J. Bale, Werner Jaschke: Virtual 3D planning of corrective osteotomy and computer-aided manufacturing of a repositioning device. *CARS 2003*: 1304
- [9] V. Zdravkovic, R. Bilic. Computer-assisted preoperative planning (CAPP) in orthopaedic surgery. *Comput Methods Programs Biomed*. 32(2):141-6. 1990